TU Delft

Delft University of Technology

Document Version
Final published version

Licence
Dutch Copyright Act (Article 25fa)

Citation (APA)
Ghezelbash, A., Prosperi, A., Sharma, S., D'Altri, A. M., Rots, J. G., & Messali, F. (2026). High-Fidelity Implicit Block-Based Numerical Modeling of Out-of-Plane Behavior in Unreinforced Masonry Walls with Pre-existing Settlement-Induced Damages. In S. Saloustros, & K. Beyer (Eds.), *Structural Analysis of Historical Constructions: SAHC 2025, Volume 1* (pp. 1007-1024). (RILEM Bookseries; Vol. 64). Springer Nature. https://doi.org/10.1007/978-3-032-13469-1_80

Important note
To cite this publication, please use the final published version (if applicable).
Please check the document version above.

Copyright
In case the licence states "Dutch Copyright Act (Article 25fa)", this publication was made available Green Open Access via the TU Delft Institutional Repository pursuant to Dutch Copyright Act (Article 25fa, the Taverne amendment). This provision does not affect copyright ownership.
Unless copyright is transferred by contract or statute, it remains with the copyright holder.

Sharing and reuse
Other than for strictly personal use, it is not permitted to download, forward or distribute the text or part of it, without the consent of the author(s) and/or copyright holder(s), unless the work is under an open content license such as Creative Commons.

Takedown policy
Please contact us and provide details if you believe this document breaches copyrights.
We will remove access to the work immediately and investigate your claim.

This work is downloaded from Delft University of Technology.

High-Fidelity Implicit Block-Based Numerical Modeling of Out-of-Plane Behavior in Unreinforced Masonry Walls with Pre-existing Settlement-Induced Damages

Amirhossein Ghezelbash[1](✉), Alfonso Prosperi[1], Satyadhrik Sharma[1], Antonio Maria D'Altri[2], Jan G. Rots[1], and Francesco Messali[1]

[1] Department of Materials, Mechanics, Management and Design, Faculty of Civil Engineering and Geosciences, Delft University of Technology, 2628 CN Delft, The Netherlands
A.Ghezelbash@tudelft.nl

[2] Department of Civil, Chemical, Environmental, and Materials Engineering, University of Bologna, 40126 Bologna, Italy

Abstract. This paper investigates settlement-induced damages in unreinforced masonry (URM) walls using a high-fidelity block-based numerical modeling approach. The research aims to address gaps in the understanding of settlement effects on URM walls with flanges, particularly with respect to their seismic out-of-plane (OOP) behavior. A parametric study is conducted on four wall specimens with varying geometries, boundary conditions, and settlement scenarios, including symmetric and asymmetric patterns. The numerical models are developed via a high-fidelity block-based finite element method that simulates masonry using expanded blocks connected by zero-thickness joints, allowing for detailed analysis of cracking patterns and damage mechanisms. Different damage states, from no visible cracks to near-collapse conditions, are identified in the response of the walls and are used as initial conditions for subsequent monotonic static pushover OOP loading. The results highlight the significant influence of settlement-induced pre-damages on the OOP response of URM walls, with varying degrees of impact observed across different specimen configurations. The findings underscore the importance of considering even "light" settlement-induced pre-damages when assessing the seismic performance of URM structures, particularly in subsidence-prone regions. Under symmetric hogging, such pre-damage level can reduce OOP stiffness and peak strength by up to 41% and 20%, respectively. This study lays the groundwork for future investigations into the seismic behavior of pre-damaged masonry structures under dynamic loading and offers valuable insights for the development of more accurate assessment and mitigation strategies for buildings subjected to settlement deformations.

Keywords: Unreinforced Masonry · Numerical Modeling · Settlement Pre-Damage · Out-of-Plane Behavior · Parametric Study

© The Author(s), under exclusive license to Springer Nature Switzerland AG 2026
S. Saloustros and K. Beyer (Eds.): SAHC 2025, RILEM Bookseries 64, pp. 1007–1024, 2026.
https://doi.org/10.1007/978-3-032-13469-1_80

1 Introduction

Ground settlement refers to the vertical movement of the ground [1] and can be caused by natural phenomena as well as man-made drivers such as construction, mining, excavation, and tunnelling [2–5]. The ground settlement represents an issue, particularly in subsidence areas, such as the Netherlands, with long-term (decades or centuries) ground deformations [6–8]. Differential settlements, which result from uneven ground deformations, can cause structures to sink, tilt, or crack [9–13]. Unreinforced masonry (URM) buildings, which are widespread in the Netherlands, are especially vulnerable to subsidence due to their quasi-brittle nature [14] as well as the use of shallow foundations [15]. The damage from ground settlement not only results in significant social, economic, and cultural losses but also entails complex and costly repairs of affected structures [16]. Hence, research is needed to predict and mitigate the impacts of land subsidence.

Only a few experimental studies on the effects of settlement on the behavior of URM structures have been conducted [17–24] due to the practical and financial constraints of replicating the complex boundary conditions required for the tests. Hence, numerical analyses have been used as a cost-effective alternative for studying URM structures undergoing settlement. However, despite the significant contributions to the understanding of the phenomenon, numerical studies also adopt simplifying assumptions and idealized conditions. For example, they often model of masonry via continuum [4, 25–34] or macro-elements [35, 36] which do not allow accurate prediction of cracking [37]. A few studies, although adopting higher-fidelity micro- or meso-scale block-based approaches, either consider cases with simplified mechanical behaviors such as rigid blocks and dry joints [19, 21, 38, 39] or, when studying regular masonry, model single walls or façades in 2D [24, 40–43] and overlook or simplify the influence of perpendicular return walls (also called flanges) on settlement. Moreover, studies do not investigate the effect of settlement as source of pre-damage, which influences the wall behaviors under subsequent loads such as earthquakes [34, 44].

To address the aforementioned knowledge gaps, this research investigates the influence of different levels of settlement-induced pre-damage on the OOP seismic response of URM return walls. A high-fidelity 3D block-based finite element model, developed in [45] and extended in [46, 47] to the dynamic regime, is employed. This paper presents the first phase of this study, focusing on simulating settlement-induced damages and identifying initial conditions to be used in subsequent OOP loading analyses. Section 2 describes the wall specimens, including their geometry, material properties, and boundary and loading conditions. Section 3 discusses settlement simulations, highlighting crack patterns under different settlement profiles. Section 4 introduces the methodology for identifying damage states related to settlement, which will serve as initial conditions for the subsequent OOP analyses. Section 5 presents preliminary results of the OOP simulations incorporating settlement-induced pre-damage. Finally, Sect. 6 summarizes the key findings and outlines directions for future research.

2 Modeling Settlement in URM Walls

In this study, the wall specimens listed in Table 1 are simulated using the finite element analysis software Abaqus [48]. The specimens consist of four return walls with varying geometries and boundary conditions. Each specimen is labelled as 'iSX,' where 'i' denotes the number of supported edges (3 or 4), and 'X' indicates the presence of openings ('O' for opening walls and 'S' for solid walls). Two walls feature window openings, while the other two are solid. Within each pair, one wall is supported at three edges (the back of the return walls and the base), and the other is supported at all edges, achieved by placing a rigid beam on top of the main panel. The walls are subjected to five settlement patterns, including symmetric and asymmetric hogging and sagging.

Table 1. Overview of the wall specimens considered in the parametric study.

Specimen Name	Top Edge Constraint	Opening Type	Pre-Compression		Settlement Scenario		
			Main Panel	Flanges	Sym[a]	Asym[b]	Rev Asym[c]
3SS	–	–	0.05 MPa	0.25 MPa	Hog[d]	Hog, Sag[e]	–
4SS	Beam	–	0.25 MPa	0.25 MPa	Hog	Hog, Sag	–
3SO	–	Window	0.05 MPa	0.25 MPa	Hog	Hog, Sag	Hog, Sag
4SO	Beam	Window	0.25 MPa	0.25 MPa	Hog	Hog, Sag	Hog, Sag

[a] Symmetric, [b] Asymmetric, [c] Reversed Asymmetric, [d] Hogging, [d]Sagging

2.1 Geometry of Wall Specimens

Figure 1 shows the geometry of numerical models, focusing on the 4SO (4-side Supported Opening) wall, which features the most detailed geometry. The wall dimensions are based on experimental tests [49] and simulations [47] of single-leaf walls typical in Dutch houses. The walls are constructed using Calcium Silicate bricks measuring 212 $\times$ 71 $\times$ 102 mm^3 (length $\times$ height $\times$ thickness) with 10-mm thick mortar layers. The main panel measures 3978 $\times$ 2754 $\times$ 102 mm^3, with 994 mm long flanges matching its height and thickness. In the 3SO/4SO walls, an asymmetrical window with dimensions of 1776 $\times$ 1620 mm2 (length $\times$ height) covers 26% of the main panel surface, positioned 555 mm from the interior side of the left flange and 567 mm above the lowest horizontal mortar joint. A two-brick-row high lintel is placed on top of the windows extending from each side by half the length of a brick. The top beam in the 4SS/4SO walls spans over the length of the wall, without extending to the flanges. Finally, the walls rest on a solid base, matching their planar shape.

2.2 Mechanical Behaviors and Material Properties

The high-fidelity block-based modeling approach of [45] is used to simulate the walls, representing masonry as expanded blocks connected by zero-thickness joints. This approach enables detailed simulation of both global and local masonry failures. The modeling approach has been adopted to simulate experiments of walls [19] and wallets [21] under non-uniform settlement with satisfactory accuracy in terms reproducing crack pattern evolution; the results are omitted due to space constraints.

The constitutive behaviors of the expanded blocks and the joints are briefly outlined herein. More detailed descriptions can be found in [45, 46]. The expanded blocks are extended to $222 \times 81 \times 102$ mm^3 (length $\times$ height $\times$ thickness) to account for mortar thickness and are discretized into an array of $4 \times 2 \times 2$ eight-node elements. Their uniaxial behavior, representing the response of masonry wallets in compression and units (bricks here) in tension, is modeled using the Concrete Damaged Plasticity (CDP) model [50, 51], and is projected to 3D space using the Drucker-Prager multi-yield surface [51]. The zero-thickness joints, representing the mortar layers and the masonry-mortar bond, exhibit cohesive tensile behavior and elastic overclosure normal to their plane, while their in-plane response is characterized by a non-dilatant isotropic cohesive-frictional shear mechanism.

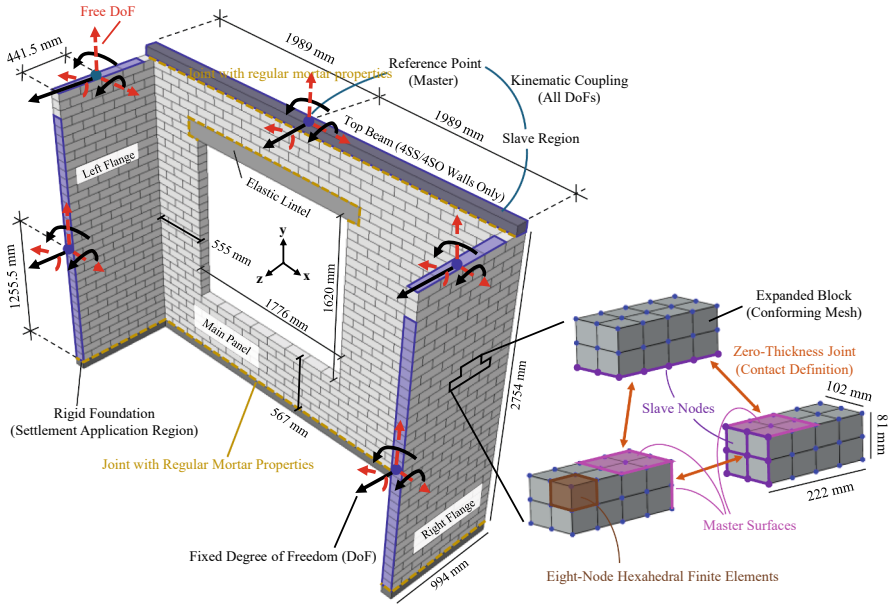


Fig. 1. Geometry and boundary conditions of the numerical models (4SO Wall), and overview of the high-fidelity block-based masonry modeling approach.

Input parameters for the constitutive models are provided in Table 2. Except for those defining the CPD response [52–54], the values are obtained from numerical models [55, 56] calibrated against experimental tests [57] on Calcium Silicate URM walls

used in Dutch residential construction [58]. The base, top beam (4SS/4SO walls), and lintel (3SO/4SO walls) are assigned the same elastic properties as the expanded blocks, although the base and beam are later made rigid (see Sect. 2.4).

Table 2. Inputs for the constitutive mechanical behaviors. Details can be found in [45, 46].

Expanded blocks							
Elastic		CDP parameters		Compressive		Tensile	
E_m	4800	ψ	10°	f'_m	6.35 MPa	f_{bt}	1.83 MPa
ν_m	0.16	ϵ	0.1	ε_{mp}	0.004	ε_{btk}	0.004
ρ_m	1708 kg/m^3	f_{b0}/f_{c0}	1.16	ε_{mk}	0.016		
		ρ	2/3				
Zero-thickness joints (vertical and horizontal joints are modeled identically)							
Overclosure		Cohesive tensile		Cohesive shear		Frictional shear	
K_{no}	221 N/mm^3	k_{nt}	221 N/mm^3	k_s	87 N/mm^3	tan ϕ	0.57
		f_t	0.096 MPa	c	0.11 MPa	δ_e	0.001 mm
		u_k	0.3 mm	δ_k	0.3 mm		

2.3 Loading Procedure

The loading sequence of each specimen begins with applying self-weight, followed by vertical loading (or overburden) applied as pressure on the top surface of the wall, and then the settlement as imposed vertical displacements of the base. All loads are applied incrementally via the static (not influenced by loading duration) implicit solver in Abaqus with automatic incrementation accounting for geometric and material non-linearity; default settings and a small maximum incrementation size are used to ensure numerical stability and prevent divergence problems.

The walls are assumed to be located at the bottom floor of a two-story building and experiencing 0.25 MPa overburden. However, different vertical loading schemes are considered (see Table 1) to align them with their corresponding boundary conditions. For 4SS/4SO walls, the 0.25 MPa pressure is applied uniformly to their whole top surface, assuming a bi-directional spanning rigid diaphragm. For the 3SS/3SO walls a unidirectional diaphragm is assumed, resulting in a smaller (0.05 MPa) overburden acting on their main panels, which corresponds then only to the weight of the structural components (such as walls) sitting on the top of the panels.

Five 2D (vertical IP) settlement profiles, including one symmetric hogging (Fig. 2a), two asymmetric sagging and hogging (Fig. 2b), and two reversed asymmetric profiles (Fig. 2c) are applied. The reversed profiles are only used for 3SO/4SO walls to assess the impact of window opening asymmetry. These settlement profiles are generated following [34, 59] based on the methodology proposed by [60] using the Gaussian normal distribution curve (Fig. 2d). The profiles are applied incrementally up to a maximum angular distortion (defined in [61]) of $\beta = 50‰$ (1/20), or until the walls collapse (i.e., fail to gain equilibrium). The final value of the applied β ensures that the settlement is large enough to reveal all possible crack paths of the specimens. The portions of base beneath the flanges are displaced as much as their corresponding ends of the main panel, neglecting settlement variations in the z-direction (studied in [62]), due to the short flange lengths. The effects of soil-structure interaction are not modeled [32], and the angular distortions experienced at the base are conservatively assumed to be equal to those recorded from the soil beneath it.

2.4 Boundary Conditions

The boundary conditions used in the simulations are illustrated in Fig. 1. These conditions are designed to accommodate both settlement and out-of-plane (OOP) analyses. To enable OOP loading, the back and top of the flanges are connected to a reference point each, simulating boundary elements that constrain the flanges during pushover analysis. The connections use kinematic coupling, constraining all degrees of freedom (DoFs) of the target surfaces to the movements of their corresponding reference points. Following [47, 49], the coupling in the flange-backs extends from the bottom joint to three block rows below the top, while at the flange-tops, it spans from the back of each flange up to one block before the edge of the main panel. In 4SS/4SO walls, the top beam is also coupled to a reference point, positioned at the wall's top edge and mid-length, to make it behave rigidly.

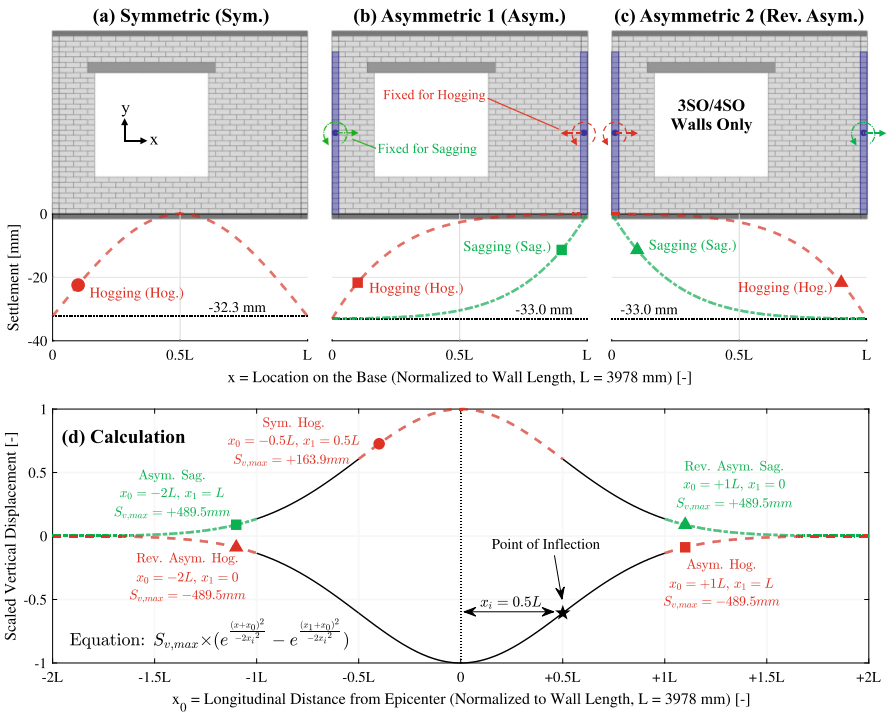


Fig. 2. Vertical displacement profiles applied at the base of the walls for settlement loading: Symmetric (a), Asymmetric (b), and Reversed Asymmetric (c) displacement profiles scaled to angular distortion of 50‰, and their calculation from the Gaussian bell curve (d).

The main panel aligns to the x-y plane and the flanges extend along the positive z-axis (Fig. 1). During all loading steps, the reference points are allowed to only move along the x- and y-axes and rotate around the z-axis, preventing their OOP movement and rocking as well as torsion. The base is fully constrained at all its nodes during gravity and pre-compression loading but allowed to move vertically during settlement to apply displacement profiles, hence, acting rigidly and only deforming as prescribed. To prevent rigid body motion and enforce cracking of the specimens under the asymmetric settlement, the back of the flange located at the zero-z-rotation end of each asymmetric profile is constrained against movement along the x-axis and rotation about the z-axis. For instance, during asymmetric hogging or sagging (Fig. 2b), the right or left flange is, respectively, constrained.

3 Crack Patterns Due to the Different Settlement Shapes

The deformed shapes of the walls at the end of the settlement application are presented in Fig. 3, illustrating their crack patterns. Walls subjected to hogging exhibit distributed damage, including vertical and diagonal cracks in the main panels (3SS/4SS) and large piers (3SO/4SO), diagonal cracks at the corners of openings (3SO/4SO), and flange detachment from the base. In contrast, sagging-induced damages are more localized,

primarily concentrated at the bottom mortar joint and panel-flange connections. Additionally, the lower horizontal confinement allows horizontal and stepped cracking of the bottom pier in 3SO/4SO walls. A notable sensitivity to the asymmetric settlement direction is observed in 3SO/4SO walls, where reversed profiles lead to greater damage propagation due to the mobilization of the larger (right) pier. Walls under asymmetric hogging display similar crack patterns to those under symmetric settlement, except for the 4SS wall, where a single dominant crack forms instead of two. The primary distinction between symmetric and asymmetric settlement cases is that the latter reaches its final cracked configuration at significantly larger distortions, up to twice as much (see Sect. 4).

4 Quantification of the Damage Severity

Different damage states are identified to serve as initial conditions for OOP loading in the upcoming parametric study. The five different states, listed in Table 3, are adapted from [63–66] and labeled as "DSi," where "i" ranges from 0 to 4, reflecting increasing damage severity. It should be noted that DS4, which approximately corresponds to the wall conditions shown in Fig. 3, is not included in the following parametric studies as walls with such damage are supposed to be demolished, reconstructed, or repaired instead of undergoing subsequent seismic events [63–65].

Each damage state is traditionally identified by the width for a single representative crack (C_w) [63–65], as detailed in Table 3. Alternatively, the scalar damage parameter (Ψ), proposed in [67], is utilized since prior studies [68] have shown that associating a single crack width with a damage state may not be sufficient to assess the damage severity. Ψ is calculated via Eq. (1) based on the number (n), length ($C_{L,i}$), and width ($C_{w,i}$) of the cracks. In the equation, $C_{w,i}$ (in mm) is calculated as the maximum width across the crack length, combining shear and opening components. All cracks, including those at the base and at the wall-flange connections, are considered in the calculation of Ψ. The range of Ψ values recommended in [15] is used to categorize the damage states in this study.

$$\Psi = 2n^{0.15}\left(\frac{\sum_{i=1}^{n} C_{L,i}C_{w,i}^{2}}{\sum_{i=1}^{n} C_{L,i}C_{w,i}}\right)^{0.3} \tag{1}$$

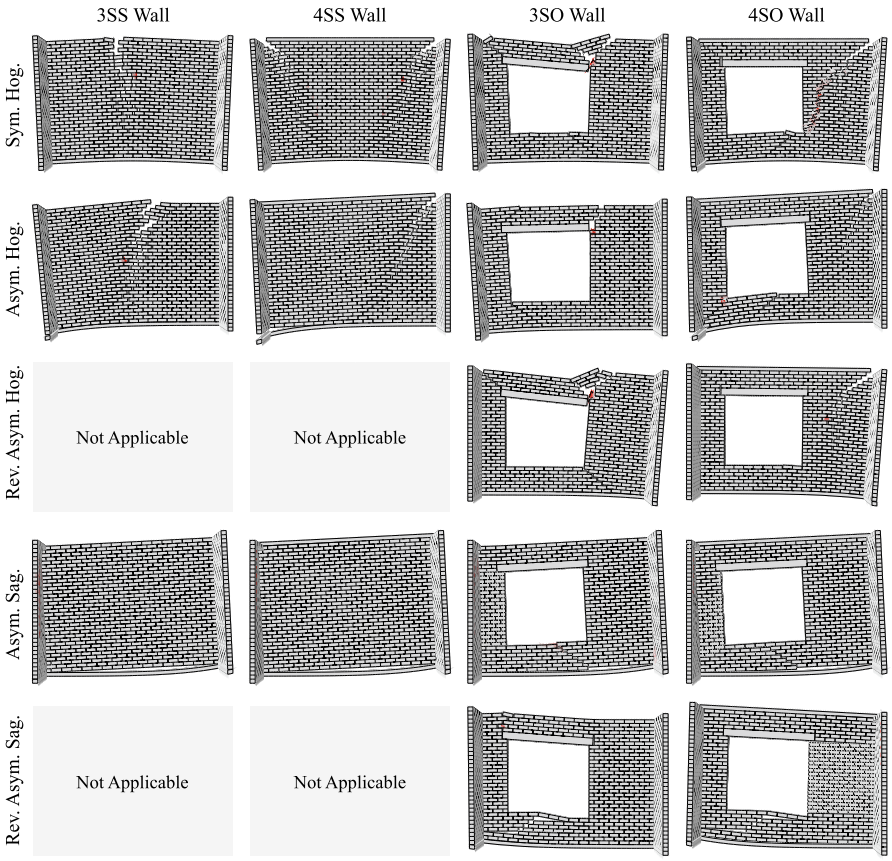


Fig. 3. Final crack pattern of all wall specimens under settlement loading. Tensile damage in the blocks (i.e., cracks in the bricks) is highlighted in red. The deformed shapes are magnified with various scales for clear visualization of the crack paths.

Table 3. Criteria adopted for identification of settlement-induced damage states.

Damage Classification				C_w [64, 65]	Ψ [15]
State	Class [63]	Description	Repair [66]		
DS0	No Damage	–	–	–	–
DS1	Light	First Visible Cracks	Easy	1–5 mm	2.5–3.5
DS2	Moderate	Increased Damages	Medium	5–15 mm	3.5–4.5
DS3	Severe	Full Crack Pattern	Extensive	15–25 mm	4.5–5.5
DS4	Near Collapse[a]	Large Deformations	Rebuild	>25 mm	>5.5

[a] Also known as Very Severe, is not considered in the following parametric study

Figure 4 shows the crack evolution from DS1 to DS3 for walls under symmetric hogging, and the values of applied angular distortion β, the maximum $C_{w,i}$ (indicated as $C_{w,max}$), and Ψ computed for each damage state. To identify the damage states, the deformed shapes of the walls are examined at every 0.625‰ (1/1600) increment of applied angular distortion. The first instances in the loading history where Ψ falls in the expected range of a given damage state (Table 3) are reported.

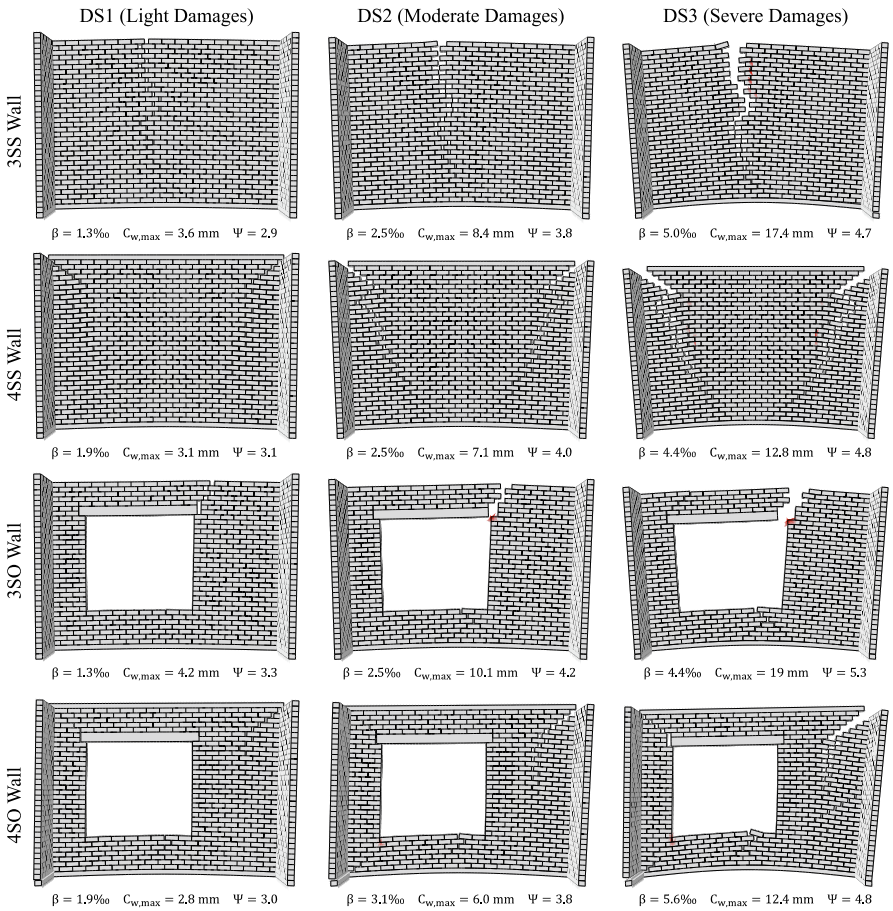


Fig. 4. Damage states identified for wall specimens under symmetric hogging. Deformed shapes are ×20 magnified. Block tensile damages (i.e., brick cracks) are highlighted in red. The β is the value of "applied angular distortion" at which the damage state is identified.

The angular distortions at which light (DS1) to severe (DS3) damages appear in different specimens and settlement scenarios are listed in Table 4. Symmetric hogging is the most severe settlement profile, reaching different damage states at lower angular distortions compared to the other profiles, showing low distortion thresholds in line with previous finding [59]. It should be observed, though, that such low values might also be

caused by the protocol followed for applying settlement, with the point of inflection in the Gaussian bell assumed at a distance from the epicenter equal to half the wall length ($x_i = L/2$), whereas in reality it can be further away and larger distortions may be needed for different damage states [15].

Both asymmetric hogging and sagging settlements reach DS3 at very large angular distortions (8.1–18.1‰, or 1/125-55) unrealistic compared to the real-world limit values in the literature (up to 3.3‰ or 1/300 [63, 67]), suggesting that such settlement profile are unable to cause large damage in the walls if the structures are rehabilitated upon reaching practical distortions. The difference between asymmetric hogging and sagging scenarios varies based on geometry and boundary conditions of the walls: the 3SS/4SS show faster damage progression under asymmetric hogging, while the 3SO/4SO walls show similar sensitivity to both asymmetric hogging and sagging. This is determined by the lower horizontal confinement in opening walls, allowing more internal deformation and crack propagation (at the bottom spandrel) during sagging. Finally, in asymmetric hogging, the 3SO/4SO walls reach DS3 earlier under the reversed profile due to the mobilization of the larger pier.

Table 4. Angular distortions corresponding to light- to severe-damage states in the models.

Settlement Profile	Angular Distortion[a] [‰]											
	3SS Wall			4SS Wall			3SO Wall			4SO Wall		
	DS1	DS2	DS3	DS1	DS2	DS3	DS1	DS2	DS3	DS1	DS2	DS3
Sym. Hog.	1.3	2.5	5.0	1.9	2.5	4.4	1.3	2.5	4.4	1.9	3.1	5.6
Asym. Hog.	3.1	6.3	11.3	3.8	6.9	14.4	1.9	3.8	7.5	4.4	8.8	12.5
Rev. Asym. Hog.	–	–	–	–	–	–	1.9	3.1	6.9	3.8	5.6	8.1
Asym. Sag.	5.0	8.8	18.1	5.0	8.8	18.1	2.5	5.6	11.9	2.5	6.3	13.1
Rev. Asym, Sag.	–	–	–	–	–	–	3.1	6.3	10.0	3.1	8.1	13.1

[a] These are the angular distortions applied to the base

5 Out-of-Plane Response of Walls Pre-damaged by Settlement

This study presents foundation knowledge for further research focusing on the effects of settlement-induced pre-damages on the "dynamic" out-of-plane (OOP) response. Consequently, in this research a preliminary assessment is conducted using pushover analysis to check the feasibility of the approach. First, the specimens are given a rest time to balance residual stresses from settlement. Then, the pushover loading is achieved by applying a uniform pressure to the surface of the main panels on the side facing the flanges, pushing the panels away from the flanges. It should be noted that during OOP loading, the reference points at the flange backs and flange tops (as well as panel tops of 4OS/4SS walls) are restrained against movement in the x- and z-directions and rotation about the x- and y-axes. The base is also fixed, maintaining its deformed shape from the corresponding settlement-induced distortion. Figure 5 presents examples of OOP

pushover analyses for walls under different asymmetric hogging pre-damage states (DS0 to DS3). The OOP reaction forces in the curves of each wall are normalized to the peak non-pre-damaged OOP strength ($V_{max,DS0}$). The OOP displacements, measured at the point of maximum deflection (top of 3SS/3SO walls, mid-height of 4SS/4SO walls), are normalized to wall thickness (t = 102 mm).

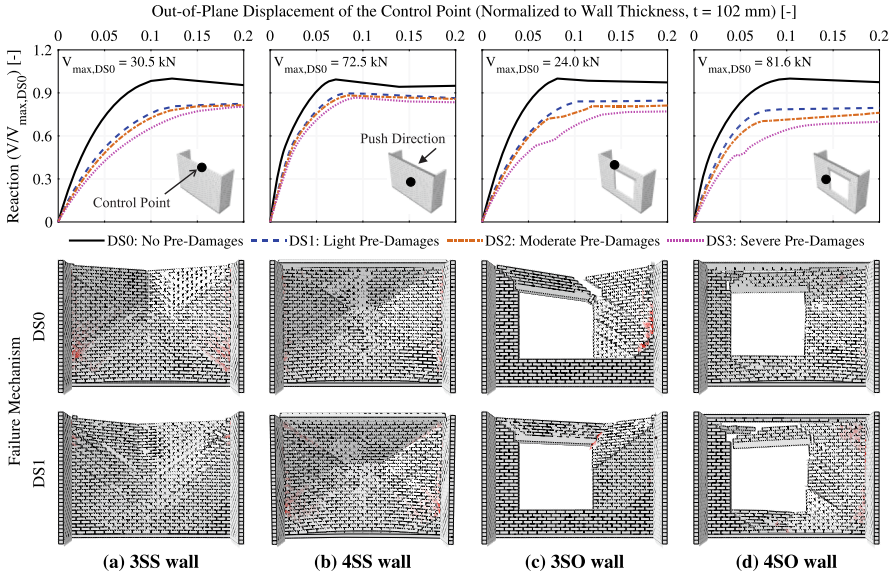


Fig. 5. Example of OOP pushover curves and failure mechanisms of wall specimens subjected symmetric hogging at different pre-damage states. The deformed shapes are magnified with various scales for clear visualization of the crack paths. The portions of the deformed shapes highlighted in red represent tensile damage in blocks (i.e., cracks in bricks).

The results show the significant impact of pre-damage on the OOP wall performance. Light pre-damage (DS1) caused by symmetric hogging is already sufficient to determine strength losses of up to 20% (4SO) and stiffness reductions of up to 41% (4SO). Deformed shapes in Fig. 5 further highlight how DS1 cracks alter the OOP failure mechanism to those wherein pre-existing settlement-induced cracks re-open instead of following the non-pre-damaged OOP failure pattern. It is observed that while the 3SS/4SS walls do not show a significant reduction of OOP performance past DS1 pre-damages, the 3SO/4SO walls continue to lose OOP strength (-28% for 4SO, compared to the strength of the non-pre-damaged wall) and stiffness (-62% for 4SO). This is because the cracks are more localized in solid walls and already well-developed at DS1, whereas crack development is more gradual in opening walls and continues until the severe pre-damage state (DS3).

Although all the walls show a similar influence of pre-damage on the OOP response, the 4SS wall exhibits the lowest sensitivity, while the 3SS, 3SO, and 4SO wall show a similar sensitivity. The 4SS wall benefits from vertical confinement due to pre-compression, preserving its integrity and contributing to its overall performance during OOP loading

despite the presence of cracks. In contrast, the 3SS and 3SO walls, lacking such confinement, experience slightly greater reductions (18% and 22% of strength, 55% and 52% of stiffness at DS3, respectively for 3SS and 3SO). The 4SO wall is considerably more affected by pre-damage compared to the 4SS wall, since the presence of the opening reduces the vertical confinement observed in the former, making the latter more vulnerable to pre-damages.

6 Conclusion

This study examines the impact of settlement-induced pre-damages on the out-of-plane (OOP) behavior of unreinforced masonry (URM) walls using a high-fidelity block-based numerical modeling approach. A parametric study is conducted on wall specimens with and without openings and top-edge support, subjected to symmetric and asymmetric hogging and sagging settlement. Settlement-induced damage states, ranging from no visible cracks to severe damage, are identified through an objective damage parameter that considers crack length, width, and number. To assess the effect of pre-damage on structural performance, OOP pushover loading is applied on the walls with different damage states. The main findings are as follows:

- Settlement damage significantly affects the OOP response of URM walls, decreasing stiffness and peak strength by up to 62% and 28%, respectively.
- Even light pre-damage results in major stiffness (41%) and strength (20%) reductions, altering the OOP failure mechanism by promoting the re-opening of settlement cracks rather than the formation of pure OOP failure modes.
- The solid wall with constrained top is less sensitive to settlement effects, benefiting from the vertical confinement provided by its vertical overburden.
- In solid walls, cracks remain largely unchanged beyond DS1, growing only in length or width, leading to most OOP performance degradation occurring early at DS1. In contrast, opening walls experience a more gradual decline in OOP response as new cracks continue to form at higher damage states.

Further research is needed to better understand how subsidence-induced pre-damage affects the seismic response of URM structures. Future studies should examine the OOP response of walls pre-damaged by different settlement profiles and consider dynamic OOP loading for more realism. Studying the long-term effects of repeated soil settlement and uplift, and improved soil-structure interaction models, is also recommended. Finally, the impact of different levels of light pre-damage (Negligible, Very Slight, and Slight [15]) on OOP response can be further explored.

Acknowledgements. This research was conducted as part of the scientific consolidation of projects funded by Nederlandse Aardolie Maatschappij (NAM) BV under contract number UI46268 “Physical testing and modeling–Masonry structures Groningen.”

References

1. Bucx, T.H.M., van Ruiten, C.J.M., Erkens, G., de Lange, G.: An integrated assessment framework for land subsidence in delta cities. Proc. Int. Assoc. Hydrol. Sci. **372**, 485–491 (2015). https://doi.org/10.5194/piahs-372-485-2015
2. Peduto, D., Ferlisi, S., Nicodemo, G., Reale, D., Pisciotta, G., Gullà, G.: Empirical fragility and vulnerability curves for buildings exposed to slow-moving landslides at medium and large scales. Landslides **14**, 1993–2007 (2017). https://doi.org/10.1007/s10346-017-0826-7
3. Saeidi, A., Deck, O., Verdel, T.: Development of building vulnerability functions in subsidence regions from empirical methods. Eng. Struct. **31**, 2275–2286 (2009). https://doi.org/10.1016/j.engstruct.2009.04.010
4. Peduto, D., Prosperi, A., Nicodemo, G., Korff, M.: District-scale numerical analysis of settlements related to groundwater lowering in variable soil conditions. Can. Geotech. J. **59**, 978–993 (2022). https://doi.org/10.1139/cgj-2021-0041
5. Stouthamer, E., Erkens, G., Cohen, K., Hegger, D., Driessen, P., Weikard, H.P., et al.: Dutch national scientific research program on land subsidence: Living on soft soils – subsidence and society. Proc. Int. Assoc. Hydrol. Sci. **382**, 815–819 (2020). https://doi.org/10.5194/piahs-382-815-2020
6. van Asselen, S., Erkens, G., Stouthamer, E., Woolderink, H.A.G., Geeraert, R.E.E., Hefting, M.M.: The relative contribution of peat compaction and oxidation to subsidence in built-up areas in the Rhine-Meuse delta, The Netherlands. Sci. Total. Environ. **636**, 177–191 (2018). https://doi.org/10.1016/j.scitotenv.2018.04.141
7. Nieuwenhuis, H.S., Schokking, F.: Land subsidence in drained peat areas of the Province of Friesland, The Netherlands. Q. J. Eng. Geol. **30**, 37–48 (1997). https://doi.org/10.1144/GSL.QJEGH.1997.030.P1.04
8. Koster, K., Stafleu, J., Stouthamer, E.: Differential subsidence in the urbanised coastal-deltaic plain of the Netherlands. Neth. J. Geosci. **97**, 215–227 (2018). https://doi.org/10.1017/njg.2018.11
9. Peduto, D., Korff, M., Nicodemo, G., Marchese, A., Ferlisi, S.: Empirical fragility curves for settlement-affected buildings: analysis of different intensity parameters for seven hundred masonry buildings in The Netherlands. Soils Found. **59**, 380–397 (2019). https://doi.org/10.1016/j.sandf.2018.12.009
10. Peduto, D., Nicodemo, G., Maccabiani, J., Ferlisi, S., D'Angelo, R., Marchese, A.: Investigating the behaviour of buildings with different foundation types on soft soils: two case studies in the Netherlands. Procedia Eng. **158**, 529–534 (2016). https://doi.org/10.1016/j.proeng.2016.08.484
11. Peduto, D., Nicodemo, G., Maccabiani, J., Ferlisi, S.: Multi-scale analysis of settlement-induced building damage using damage surveys and DInSAR data: a case study in The Netherlands. Eng. Geol. **218**, 117–133 (2017). https://doi.org/10.1016/j.enggeo.2016.12.018
12. Nicodemo, G., Peduto, D., Ferlisi, S.: Building damage assessment and settlement monitoring in subsidence-affected urban areas: case study in the Netherlands. Proc. Int. Assoc. Hydrol. Sci. **382**, 651–656 (2020). https://doi.org/10.5194/piahs-382-651-2020
13. Costa, A.L., Kok, S., Korff, M.: Systematic assessment of damage to buildings due to groundwater lowering-induced subsidence: methodology for large scale application in the Netherlands. Proc. Int. Assoc. Hydrol. Sci. **382**, 577–582 (2020). https://doi.org/10.5194/piahs-382-577-2020
14. Frankie, T.M., Gencturk, B., Elnashai, A.S.: Simulation-based fragility relationships for unreinforced masonry buildings. J. Struct. Eng. **139**, 400–410 (2013). https://doi.org/10.1061/(ASCE)ST.1943-541X.0000648

15. Prosperi, A.: Modelling of subsidence induced damage to masonry buildings: influence of soil heterogeneity on settlement and development of fragility. Ph.D. thesis. Delft University of Technology (2025)
16. Willemsen, W., Kok, S., Kuik, O.: The effect of land subsidence on real estate values. Proc. Int. Assoc. Hydrol. Sci. **382**, 703–707 (2020). https://doi.org/10.5194/piahs-382-703-2020
17. Dalgic, K.D., Gulen, B., Liu, Y., Acikgoz, S., Burd, H., Marasli, M., et al.: Masonry buildings subjected to settlements: half-scale testing, detailed measurements, and insights into behaviour. Eng. Struct. **278**, 115233 (2023). https://doi.org/10.1016/j.engstruct.2022.115233
18. Giardina, G., Marini, A., Hendriks, M.A.N., Rots, J.G., Rizzardini, F., Giuriani, E.: Experimental analysis of a masonry façade subject to tunnelling-induced settlement. Eng. Struct. **45**, 421–434 (2012). https://doi.org/10.1016/j.engstruct.2012.06.042
19. Bui, T.T., Limam, A., Sarhosis, V., Hjiaj, M.: Discrete element modelling of the in-plane and out-of-plane behaviour of dry-joint masonry wall constructions. Eng. Struct. **136**, 277–294 (2017). https://doi.org/10.1016/j.engstruct.2017.01.020
20. Karanikoloudis, G., Serra, J., Lourenço, P.B.: Experimental tests and analytical strength models of differential settlements on unreinforced masonry piers and spandrel specimens. J. Build. Eng. **89**, 109192 (2024). https://doi.org/10.1016/j.jobe.2024.109192
21. Portioli, F., Cascini, L.: Large displacement analysis of dry-jointed masonry structures subjected to settlements using rigid block modelling. Eng. Struct. **148**, 485–496 (2017). https://doi.org/10.1016/j.engstruct.2017.06.073
22. Beyer, K.: Peak and residual strengths of brick masonry spandrels. Eng. Struct. **41**, 533–547 (2012). https://doi.org/10.1016/j.engstruct.2012.03.015
23. Meoni, A., Mattiacci, M., D'Alessandro, A., Virgulto, G., Buratti, N., Ubertini, F.: Automated damage detection in masonry structures using cointegrated strain measurements from smart bricks: application to a full-scale building model subjected to foundation settlements under changing environmental conditions. J. Build. Eng. **100**, 111749 (2025). https://doi.org/10.1016/j.jobe.2024.111749
24. Son, M., Cording, E.J.: Estimation of building damage due to excavation-induced ground movements. J. Geotech. Geoenviron. Eng. **131**, 162–177 (2005). https://doi.org/10.1061/(ASCE)1090-0241(2005)131:2(162)
25. Giardina, G., van de Graaf, A.V., Hendriks, M.A.N., Rots, J.G., Marini, A.: Numerical analysis of a masonry façade subject to tunnelling-induced settlements. Eng. Struct. **54**, 234–247 (2013). https://doi.org/10.1016/j.engstruct.2013.03.055
26. Burd, H.J., Houlsby, G.T., Augarde, C.E., Liu, G.: Modelling tunnelling-induced settlement of masonry buildings. Proc. Inst. Civil Eng. Geotech. Eng. **143**, 17–29 (2000). https://doi.org/10.1680/geng.2000.143.1.17
27. Netzel, H.D.: Building response due to ground movements. Delft University of Technology (2009)
28. Yiu, W.N., Burd, H.J., Martin, C.M.: Finite-element modelling for the assessment of tunnel-induced damage to a masonry building. In: Tunnelling in the Urban Environment, pp. 59–73. ICE Publishing (2018). https://doi.org/10.1680/tue.63778.059
29. Rots, J.G., Korswagen, P.A., Longo, M.: Computational modelling checks of masonry building damage due to deep subsidence. Delft, The Netherlands (2021)
30. Burd, H.J., Yiu, W.N., Acikgoz, S., Martin, C.M.: Soil-foundation interaction model for the assessment of tunnelling-induced damage to masonry buildings. Tunn. Undergr. Space Technol. **119**, 104208 (2022). https://doi.org/10.1016/j.tust.2021.104208
31. Prosperi, A., Longo, M., Korswagen, P.A., Korff, M., Rots, J.G.: Accurate and efficient 2D modelling of historical masonry buildings subjected to settlements in comparison to 3D approaches. In: International Conference on Structural Analysis of Historical Constructions, Kyoto, Japan (2023)

32. Longo, M., Sousamli, M., Korswagen, P.A., van Staalduinen, P., Rots, J.G.: Sub-structure-based 'three-tiered' finite element approach to soil-masonry-wall interaction for light seismic motion. Eng. Struct. **245**, 112847 (2021). https://doi.org/10.1016/j.engstruct.2021.112847
33. Prosperi, A., Longo, M., Korswagen, P.A., Korff, M., Rots, J.G.: Sensitivity modelling with objective damage assessment of unreinforced masonry façades undergoing different subsidence settlement patterns. Eng. Struct. **286**, 116113 (2023). https://doi.org/10.1016/j.engstruct.2023.116113
34. Korswagen, P.A., Longo, M., Prosperi, A., Rots, J.G., Terwel, K.C.: Modelling of Damage in Historical Masonry Façades Subjected to a Combination of Ground Settlement and Vibrations, pp. 904–917 (2024). https://doi.org/10.1007/978-3-031-39603-8_73
35. Nicodemo, G., Peduto, D., Ferlisi, S.: Numerical analysis of the behaviour of masonry buildings undergoing differential settlements. In: 17th European Conference on Soil Mechanics and Geotechnical Engineering, Reykjavik, Iceland (2019)
36. Ferlisi, S., Nicodemo, G., Peduto, D., Negulescu, C., Grandjean, G.: Deterministic and probabilistic analyses of the 3D response of masonry buildings to imposed settlement troughs. Georisk: Assess. Manag. Risk Eng. Syst. Geohazards **14**, 260–279 (2020). https://doi.org/10.1080/17499518.2019.1658880
37. D'Altri, A.M., Sarhosis, V., Milani, G., Rots, J., Cattari, S., Lagomarsino, S., et al.: Modeling strategies for the computational analysis of unreinforced masonry structures: review and classification. Arch. Comput. Methods Eng. **27**, 1153–1185 (2020)
38. Gagliardo, R., Portioli, F.P.A., Cascini, L., Landolfo, R., Lourenço, P.B.: A rigid block model with no-tension elastic contacts for displacement-based assessment of historic masonry structures subjected to settlements. Eng. Struct. **229**, 111609 (2021). https://doi.org/10.1016/j.engstruct.2020.111609
39. Portioli, F.P.A., Cascini, L., Landolfo, R., Lourenço, P.B.: An optimization-based rigid block modeling approach to seismic assessment of dry-joint masonry structures subjected to settlements. Soil Dyn. Earthq. Eng. **166**, 107760 (2023). https://doi.org/10.1016/j.soildyn.2023.107760
40. Chen, X., Wang, X., Wang, H., Agrawal, A.K., Chan, A.H.C.: Simulating the failure of masonry walls subjected to support settlement with the combined finite-discrete element method. J. Build. Eng. **43**, 102558 (2021). https://doi.org/10.1016/j.jobe.2021.102558
41. Son, M., Cording, E.J.: Evaluation of building stiffness for building response analysis to excavation-induced ground movements. J. Geotech. Geoenviron. Eng. **133**, 995–1002 (2007). https://doi.org/10.1061/(ASCE)1090-0241(2007)133:8(995)
42. Hong, L.T., Laefer, D.F.: Micro vs. macro models for predicting building damage underground movements. In: The International Conference on Computational Solid Mechanics, Hochiminh City, Vietnam (2008)
43. D'Altri, A.M., Pereira, M., de Miranda, S., Glisic, B.: Simulation-driven machine learning for real-time damage prognosis in masonry structures. Int. J. Mech. Sci. **289**, 110055 (2025). https://doi.org/10.1016/j.ijmecsci.2025.110055
44. Korswagen, P.A., Longo, M., Meulman, E., Rots, J.G.: Crack initiation and propagation in unreinforced masonry specimens subjected to repeated in-plane loading during light damage. Bull. Earthq. Eng. **17**, 4651–4687 (2019). https://doi.org/10.1007/s10518-018-00553-5
45. D'Altri, A.M., Messali, F., Rots, J., Castellazzi, G., de Miranda, S.: A damaging block-based model for the analysis of the cyclic behaviour of full-scale masonry structures. Eng. Fract. Mech. **209**, 423–448 (2019). https://doi.org/10.1016/j.engfracmech.2018.11.046
46. Ghezelbash, A., D'Altri, A.M., Sharma, S., Lourenço, P.B., Rots, J.G., Messali, F.: A block-based numerical strategy for modeling the dynamic out-of-plane behavior of unreinforced brick masonry walls. Meccanica **60**, 2069–2105 (2024). https://doi.org/10.1007/s11012-024-01899-8

47. Ghezelbash, A., Sharma, S., D'Altri, A.M., Lourenço, P.B., Rots, J.G., Messali, F.: Challenges in high-fidelity implicit block-based numerical simulation of dynamic out-of-plane two-way bending in unreinforced brick masonry walls. Earthq. Eng. Struct. Dyn. **54**, 1836–1858 (2025). https://doi.org/10.1002/eqe.4337
48. Hibbitt, D., Karlsson, B., Sorensen, P.: Abaqus/CAE User's Manual. USA: Dassault Systèmes SE (2011)
49. Graziotti, F., Tomassetti, U., Sharma, S., Grottoli, L., Magenes, G.: Experimental response of URM single leaf and cavity walls in out-of-plane two-way bending generated by seismic excitation. Constr. Build. Mater. **195**, 650–670 (2019). https://doi.org/10.1016/j.conbuildmat.2018.10.076
50. Lee, J., Fenves, G.L.: Plastic-damage model for cyclic loading of concrete structures. J. Eng. Mech. **124**, 892–900 (1998). https://doi.org/10.1061/(ASCE)0733-9399(1998)124:8(892)
51. Lubliner, J., Oliver, J., Oller, S., Oñate, E.: A plastic-damage model for concrete. Int. J. Solids Struct. **25**, 299–326 (1989). https://doi.org/10.1016/0020-7683(89)90050-4
52. Milani, G., Valente, M., Alessandri, C.: The narthex of the Church of the Nativity in Bethlehem: a non-linear finite element approach to predict the structural damage. Comput. Struct. **207**, 3–18 (2018). https://doi.org/10.1016/j.compstruc.2017.03.010
53. Scacco, J., Ghiassi, B., Milani, G., Lourenço, P.B.: A fast modeling approach for numerical analysis of unreinforced and FRCM reinforced masonry walls under out-of-plane loading. Compos. B Eng. **180**, 107553 (2020). https://doi.org/10.1016/j.compositesb.2019.107553
54. Castellazzi, G., D'Altri, A.M., de Miranda, S., Ubertini, F.: An innovative numerical modeling strategy for the structural analysis of historical monumental buildings. Eng. Struct. **132**, 229–248 (2017). https://doi.org/10.1016/j.engstruct.2016.11.032
55. Ghezelbash, A., Messali, F., Rots, J.G.: Challenges in the calibration of finite element models for the analysis of masonry structures: a comparative study. In: XVII International Conference on Computational Plasticity, Fundamentals and Applications, Barcelona, Spain (2023)
56. Ghezelbash, A., Messali, F., Rots, J.G.: Finite element micro-modelling of masonry structures: calibration and analysis challenges. In: Engineering Mechanics Institute (EMI) International Conference, Palermo, Italy (2023)
57. Messali, F., Esposito, R., Ravenshorst, G.J.P., Rots, J.G.: Experimental investigation of the in-plane cyclic behaviour of calcium silicate brick masonry walls, vol. 18. Springer, Cham (2020). https://doi.org/10.1007/s10518-020-00835-x
58. Jafari, S., Esposito, R., Rots, J.G.: From Brick to Element: Investigating the Mechanical Properties of Calcium Silicate Masonry, pp. 596–604 (2019). https://doi.org/10.1007/978-3-319-99441-3_64
59. Prosperi, A., Longo, M., Korswagen, P.A., Korff, M., Rots, J.G.: 2D and 3D modelling strategies to reproduce the response of historical masonry buildings subjected to settlements. Int. J. Archit. Herit. 1–17 (2024). https://doi.org/10.1080/15583058.2024.2325472
60. Peck, R.B.: Deep excavations and tunneling in soft ground. In: 7th International Conference on Soil Mechanics and Foundation Engineering, Mexico, Mexico, pp. 225–290 (1969)
61. Burland, J.B., Wroth, C.P.: Settlement of Buildings and Associated Damage. Hertsford, England (1975)
62. Zhao, J., DeJong, M.: Three-dimensional probabilistic assessment of tunneling induced structural damage using Monte-Carlo method and hybrid finite element model. Comput. Geotech. **154**, 105122 (2023). https://doi.org/10.1016/j.compgeo.2022.105122
63. Giardina, G.: Modelling of settlement induced building damage. Delft University of Technology (2013)
64. Burland, J.B., Broms, B.B., De Mello, V.F.B.: Behaviour of foundations and structures. In: 9th International Conference on Soil Mechanics and Foundation Engineering, Tokyo, Japan (1977)

65. Boscardin, M.D., Cording, E.J.: Building response to excavation-induced settlement. J. Geotech. Eng. **115**, 1–21 (1989). https://doi.org/10.1061/(ASCE)0733-9410(1989)115:1(1)
66. Grünthal, G.: EMS-98: European Macroseismic Scale. Luxembourg, Luxembourg (1998)
67. Quantifying the probability of light damage to masonry structures: an exploration of crack initiation and progression due to seismic vibrations on masonry buildings with existing damage. Ph.D. thesis. Delft University of Technology (2024)
68. Chen, Z.Q., Hutchinson, T.C.: Image-based framework for concrete surface crack monitoring and quantification. Adv. Civil Eng. **2010**, 1–18 (2010). https://doi.org/10.1155/2010/215295